Two-body dissipation effect in nuclear fusion reactions

Kai Wen,[*] M. C. Barton, Arnau Rios, and P. D. Stevenson
Faculty of Engineering and Physical Sciences, University of Surrey, Guildford, Surrey GU2 7XH, United Kingdom

Friction coefficients for the fusion reaction $^{16}O + ^{16}O \rightarrow ^{32}S$ are extracted based on both the time-dependent Hartree-Fock and the time-dependent density matrix methods. The latter goes beyond the mean-field approximation by taking into account the effect of two-body correlations, but in practical simulations of fusion reactions we find that the total energy is not conserved. We analyze this problem and propose a solution that allows for a clear quantification of dissipative effects in the dynamics. Compared to mean-field simulations, friction coefficients in the density-matrix approach are enhanced by about 20%. An energy dependence of the dissipative mechanism is also demonstrated, indicating that two-body collisions are more efficient at generating friction at low incident energies.

I. INTRODUCTION

For a wide range of incident energies, the collisions of two nuclei exhibit typical dissipative properties [1,2]. The kinetic energy initially residing in collective motion irreversibly converts into intrinsic nuclear excitations. This is in analogy to Brownian motion, where the kinetic energy of a Brownian particle converts into the surrounding heat bath [3,4]. Exploiting this analogy, the language of nonequilibrium statistical physics has been borrowed to describe the dissipation observed to occur in nuclear reactions since the 1980s [4,5]. The concept of friction has been introduced and widely accepted in the study of heavy ion collisions [2–4]. Various theoretical models have been developed to understand the mechanisms underlying this special dissipative process [5–10].

Among these theoretical models, the time-dependent Hartree-Fock (TDHF) approach stands out as a general theoretical framework that allows for a self-consistent quantal modeling of large amplitude nuclear collective motion [11–16]. TDHF has been extensively used in the past to study low-energy nuclear collisions [17–22]. Since this method relies on a mean-field or density-functional description of nuclear dynamics, the dissipation encoded in the dynamics is due to microscopic one-body processes [3,23,24]. By mapping the TDHF evolution to the one-dimensional Langevin equation, a method called dissipative dynamics TDHF (DD-TDHF) has also been developed to study the dissipation in nuclear fusion reactions [25–27]. Dissipative effects extracted from DD-TDHF are of a one-body type, in agreement with the idea that dissipation is caused by the exchange of nucleons across the window between the colliding nuclei [4].

The exact dynamics of a quantum many-body system is governed by equations that in principle go beyond the mean-field approach. When projected into time-local many-body density matrices, the dynamics can be expressed in terms of the so-called Bogoliubov-Born-Green-Kirkwood-Yvon (BBGKY) hierarchy [28,29]. Different levels of truncation within the hierarchy provide different descriptions of the many-body dynamics, and higher-order truncation schemes are expected to describe more accurately the time evolution of the strongly correlated systems [30–33]. The TDHF approach arises naturally as the the lowest-order truncation scheme in the BBGKY hierarchy, assuming that two- and higher-body correlations are negligible [34,35].

To go beyond the mean-field approximation, in nuclear physics another truncation scheme has been implemented to account for dynamical effects on the two-body density matrix [30,34]. This so-called time-dependent density matrix (TDDM) approach extends the TDHF method by including terms that account for the evolution of the two-body density matrix in the BBGKY hierarchy and by neglecting three-body and higher-order correlations [33,34,36–39]. The numerical cost associated with directly solving the corresponding set of TDDM coupled equations is large even with the presently available computational power.

A practical method has been suggested and applied to reduce this numerical task. One can expand the problem into a single-particle basis that evolves following a TDHF-like equation [40–42]. All the one- and two-body observables are then built up using this moving basis set, truncated at a given maximum number of states. This numerical technique facilitates the calculation significantly, and provides a conserving approximation in the sense that it formally conserves particle number as well as total energy over time [30,31,34]. It has been successfully implemented in the study of nuclear ground-state properties in a self-consistent three-dimensional setting [43,44]. However, in practical simulations of large amplitude collective motion, we find that this technique comes at the price of losing energy conservation [30], due to the incompleteness of basis. This drawback hinders a quantitative study of the dissipation mechanism in the framework of TDDM.

In this work, we present a strategy that simultaneously probes the problem of basis incompleteness and restores the conservation of energy. This strategy is implemented in a practical setting that can easily be extended to other methods and

---
[*]k.wen@surrey.ac.uk

that allows the extraction of information on dissipation in the system even if the total energy is only partially conserved. With this method, we quantify the effect of two-body dissipation in a symmetric fusion reaction of two oxygen isotopes.

The paper is organized as follows. In Sec. II, we give the formulation of the basic TDDM equations, introduce the numerical method to restore the conservation of total energy, and discuss a macroscopic reduction procedure to extract friction coefficients. We apply these methods to study dissipative process in the fusion reaction $^{16}\text{O} + {}^{16}\text{O} \leftrightarrow {}^{32}\text{S}$ in Sec. III. A summary and concluding remarks are given in Sec. IV.

II. THEORETICAL FRAMEWORK

In the application of TDDM, a full calculation of the two-body-interaction matrix requires a large numerical effort at every time step [43]. This numerical cost also increases rapidly with the number of basis states and precludes realistic applications for intermediate mass nuclei. In consequence, we have adopted the TDDM^P approximation, where only the interaction between time-reversed pairs is considered. This simplified implementation of TDDM provides a generalization of pairing dynamics and has been successfully applied to study the effect of nuclear correlations on the breakup mechanism of light nuclides [45,46]. We adopt the TDDM^P approximation in our calculation and devote the next subsection to recapitulating the basic formulation of the TDDM and TDDM^P methods. Further details can be found in references [37,46].

A. TDDM^P implementation of TDDM

The TDDM method aims at determining the time evolution of both the one-body density matrix, ρ, and two-body correlation matrix, C_2, in a self-consistent way, assuming three-body and higher-order correlations are negligible. C_2 is customarily defined as the correlated part of the two-body density matrix, $C_2 = \rho_2 - \hat{A}(\rho\rho)$, where $\hat{A}$ stands for an antisymmetrization operator.

To solve the first two equations of the BBGKY hierarchy, we chose to expand ρ and C_2 in a finite number of single-particle states, $\psi_i(\mathbf{r}, t)$, $i = 1, \ldots, N_{\text{max}}$, which evolve in time obeying a TDHF-like equation of motion,

$$i\hbar\dot{\psi}_i(\mathbf{r}, t) = \hat{h}(t, \rho)\psi_i(\mathbf{r}, t). \quad (1)$$

We note that the mean-field Hamiltonian, $\hat{h}(t, \rho)$, depends on the correlated one-body density matrix. The TDHF evolution would, instead, rely on an uncorrelated Hartree-Fock-like density. Note also that the truncation parameter N_{max} is introduced here.

In terms of this moving basis, the one-body density and two-body correlation matrices are expressed as

$$\rho(\mathbf{r_1}, \mathbf{r_{1'}}; t) = \sum_{ii'} n_{ii'}(t)\psi_i(\mathbf{r_1}, t)\psi_{i'}^*(\mathbf{r_{1'}}, t), \quad (2)$$

$$C_2(\mathbf{r_1}, \mathbf{r_2}, \mathbf{r_{1'}}, \mathbf{r_{2'}}; t) = \sum_{iji'j'} C_{iji'j'}(t)\psi_i(\mathbf{r_1}, t)\psi_j(\mathbf{r_2}, t)\psi_{i'}^*(\mathbf{r_{1'}}, t)$$

$$\times \psi_{j'}^*(\mathbf{r_{2'}}, t), \quad (3)$$

where all indices run over the whole basis set. In addition to Eq. (1), the TDDM methods solve the dynamics in terms of the time evolution of single-particle occupation numbers, $n_{ii'}(t)$, and the correlation matrix, $C_{iji'j'}(t)$:

$$i\hbar\dot{n}_{ii'}(t) = \sum_{jkl}[\langle ij|v|kl\rangle C_{kli'j} - C_{ijkl}(t)\langle kl|v|i'j\rangle], \quad (4)$$

$$i\hbar\dot{C}_{iji'j'}(t) = B_{iji'j'}(t) + P_{iji'j'}(t) + H_{iji'j'}(t), \quad (5)$$

where $\langle ij|v|kl\rangle$ is a two-body interaction matrix element. The matrix terms on the right-hand side of Eq. (5) represent different correlation mechanisms. $B_{iji'j'}$ is generally associated with the Born terms, containing the physics of direct in-medium collisions [30]. The terms $P_{iji'j'}$ and $H_{iji'j'}$ represent higher-order correlations. All these terms can be expressed as a combination of interaction matrix elements, occupation numbers, and correlation matrices [30], forming a closed set of TDDM equations.

There are two major computational bottlenecks in the practical implementation of the TDDM equations. One is calculation of the interaction matrix elements in Eq. (4), which requires in principle a loop over four different single-particle indices at every time step. The second bottleneck arises similarly in the solution of Eq. (5), which requires manipulations of a four-index tensor of size N_{max}^4 [43]. A significant reduction of the numerical cost can be achieved by the TDDM^P implementation of the TDDM equations [45,46]. In this approach, one assumes that the residual two-body interaction is dominated by time-reversed pair states, $\{i, \bar{i}\}$. One keeps only the elements of the interaction matrix between these pairs, $\langle i\bar{i}|v|j\bar{j}\rangle$, and assumes that all other matrix elements are zero. The correlation matrix C is also only formed by time-reversed pair states. The number of required matrix elements in both V and C is therefore significantly reduced. Further, the term $H_{iji'j'}$ in Eq. (5) cancels out, and Eqs. (4) and (5) reduce to

$$\dot{n}_\alpha = \frac{2}{\hbar}\sum_\gamma \text{Im}(V_{\alpha\gamma}C_{\gamma\alpha}), \quad (6)$$

$$i\hbar\dot{C}_{\alpha\beta} = V_{\alpha\beta}\left[(1 - n_\alpha)^2 n_\beta^2 - (1 - n_\beta)^2 n_\alpha^2\right]$$

$$+ \sum_\gamma V_{\alpha\gamma}(1 - 2n_\alpha)C_{\gamma\beta} - \sum_\gamma V_{\gamma\beta}(1 - 2n_\beta)C_{\alpha\gamma}. \quad (7)$$

Here, the greek indexes $\alpha, \beta, \ldots$ represent a pair of time reversed states. $V_{\alpha\beta}$ is the antisymmetric element of the interaction matrix between two pairs, $V_{\alpha\beta} = \langle \alpha\bar{\alpha}|v|\beta\bar{\beta}\rangle_A$, and $C_{\alpha\beta}$ is the corresponding two-body correlation tensor, $C_{\alpha\beta} = \langle \alpha\bar{\alpha}|C|\beta\bar{\beta}\rangle$. In a sense, the interaction adopted here can be seen as a generalized BCS interaction, and TDDM^P is akin to a superfluid time-dependent approach [45].

B. TDDM with optimized basis

The conservation of total energy is critical for the analysis of the dissipation mechanism. Without the conservation of total energy, the collective kinetic and potential energies cannot be assigned unambiguously and the quantification of dissipation processes becomes impossible.
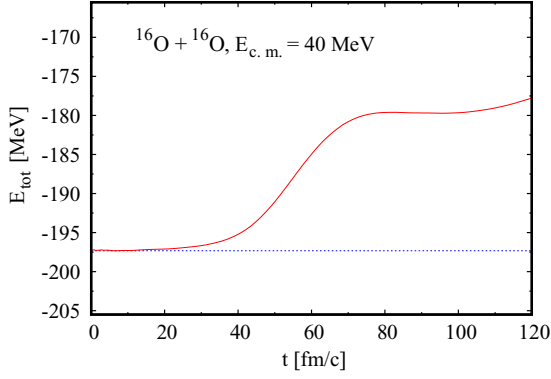
FIG. 1. Total energy of the fusion system $^{16}O + ^{16}O \rightarrow ^{32}S$ at incident $E_{c.m.} = 40$ MeV as a function of time t. The calculation is performed using the TDDM^P model. The dashed blue line indicates the constant initial energy for reference. This figure is obtained with $N_{max} = 60$.

Formally, both the TDDM and TDDM^P equations preserve the conservation of average particle number, momentum, and energy if a complete basis is present [30,45]. However, a finite basis evolving with Eq. (1) spoils the energy conservation in practical calculations [30]. The violation of energy conservation depends sensitively on the form and strength of the residual interaction, and cannot be remedied by increasing the size of the model space, N_{max}, within practical limits. Figure 1 shows an example of a TDDM^P simulation of the collision $^{16}O + ^{16}O \rightarrow ^{32}S$ at an incident energy of $E_{c.m.} = 40$ MeV. In the approaching phase, $t < 30$ fm/c, the energy is approximately conserved. A rapid increase in energy is observed in the region $30 < t < 80$ fm/c, which corresponds to the merging process: starting from the point of contact to the formation of a compact system. In this example, the total energy increases by about 18 MeV. This corresponds to a relative deviation compared to the initial value of about 10%. We take this as an indication that the moving basis that reproduces well the projectile and target nuclides in the initial state is not reliable in the rapidly evolving fusion process.

The inclusion of a complete set of basis states to simulate nuclear fusion reactions is, however, infeasible. The idea to adopt a set of moving basis whose time evolution obey TDHF-like equations is based on the expectation that this basis would to some extent satisfy the requirement of the actual solution of the full dynamics. Keeping the same motivation, we modify Eq. (1) by introducing an additional term in the mean-field Hamiltonian,

$$i\hbar \dot{\psi}_i(\mathbf{r},t) = [\hat{h}(t,\rho) + v_i'(t)]\psi_i(\mathbf{r},t). \qquad (8)$$

The gradient of the correction terms $v_i'(t)$ is related to the average momentum of each single-particle state,

$$\nabla v_i'(t) = \beta(t)\langle \psi_i(t)|\hat{p}|\psi_i(t)\rangle, \qquad (9)$$

where $\hat{p}$ is the momentum operator. $\beta(t)$ is a free parameter that allows one to fix the scale of the correction. An overall constant in v_i' will not change the result, and we choose to set it to zero.

The terms $v_i'(t)$ are designed to optimize the basis by conserving the total energy upon adjusting the parameter $\beta(t)$ at each time step. Whenever $\beta = 0$, no adjustment is necessary and the energy is conserved. A nonzero β will appear when the basis of Eq. (1) fails to conserve the total energy, with a larger β in principle indicating a worse-performing basis. Thus, $\beta(t)$ can also be seen as a proxy that quantifies to what extent the moving basis defined by Eq. (1) is satisfactory, in the sense that it provides energy conservation. We note that while v_i' depends on the orbit i, β is assumed to be the same for all orbits. Because of this orbital dependence, v_i' cannot be absorbed in a redefinition of the mean-field Hamiltonian.

To fix $\beta(t)$, the following numerical procedure is performed. At an arbitrary time, t_0, we evolve the system for one time step, Δt, in two independent ways. The first follows the TDHF-like trajectory of Eq. (1). The second follows Eq. (8), with a small $\beta(t_0) = \beta'$, which is arbitrarily set to 10^{-4} c/fm in this work. If energy is not conserved, after a time step Δt the energies of the two trajectories can be different. The total energy of the first trajectory changes from $E(t_0)$ to $E_1(t_0 + \Delta t)$, whereas the total energy of the second trajectory changes to $E_2(t_0 + \Delta t)$. When Δt, β', as well as the finally desired $\beta(t_0)$ are all small, $E_2(t_0 + \Delta t) - E_1(t_0 + \Delta t)$ is proportional to β' by a constant. $\beta(t_0)$ can be fixed using this linear relation as

$$\beta(t_0) = \beta' \frac{E_1(t_0 + \Delta t) - E(t_0)}{E_2(t_0 + \Delta t) - E_1(t_0 + \Delta t)}. \qquad (10)$$

Having obtained $\beta(t_0)$, we restart the time evolution from time t_0 following Eq. (8). With the choice of $\beta(t_0)$ above, the total energy will be conserved up to $t_0 + \Delta t$, $E(t_0 + \Delta t) = E(t_0)$. Repeating this procedure at $t_0 + \Delta t$, $t_0 + 2\Delta t \dots$, we find a constant total energy $E(t_0) = E(t_0 + \Delta t) = E(t_0 + 2\Delta t) \dots$, while repeatedly adjusting $\beta(t)$ as a function of time. The cost of performing this procedure is obviously about a factor of 2 heavier than the original solution.

This strategy provides a practical implementation of energy conserving TDDM equations. It also allows for a clear quantification of energy nonconserving dynamics whenever $\beta \neq 0$. In principle, the correction introduced in Eq. (8) should also change the form of Eqs. (4) and (5). However, our simulations indicate that $\beta(t)$ is rather small, so we keep the form of these equations unchanged.

C. Macroscopic reduction procedure

For simplicity, we consider a head-on symmetric collision along the z axis. In the center-of-mass coordinate frame, we keep the identities of both the projectile and target. In other words, the projectile and target can be identified by summing over the single-particle states that were originally ascribed to each one of them. The collective coordinate R at time t is defined as the relative distance between the center-of-masses of projectile and target,

$$R(t) = \langle \Psi(t)_{pro}|z|\Psi(t)_{pro}\rangle - \langle \Psi(t)_{tar}|z|\Psi(t)_{tar}\rangle. \qquad (11)$$

In the case of TDHF, $\Psi(t)$ represents a single Slater determinant formed of all the occupied single-particle states, ψ_i. For TDDM, the center of mass of the projectile or target can be
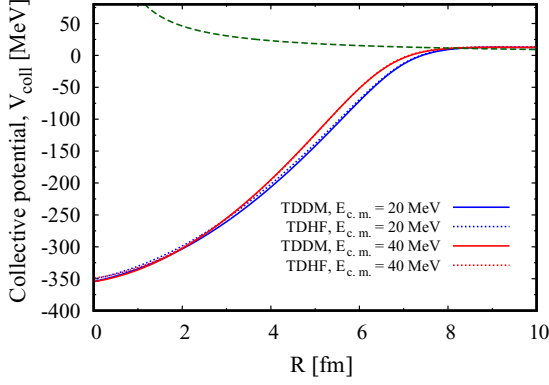
FIG. 2. Collective potential defined in Eq. (15) as a function of relative distance, R, for the fusion path in the reaction $^{16}\mathrm{O} + ^{16}\mathrm{O} \rightarrow$ $^{32}\mathrm{S}$. The solid and dotted lines indicate the results of TDDM and TDHF, respectively. The blue (lower) and red (upper) lines indicate the results at incident energies of $E_{\mathrm{c.m.}} = 20$ MeV and $E_{\mathrm{c.m.}} = 40$ MeV, respectively. The green (dashed) line shows the asymptotic Coulomb potential, $64e^2/R$, for reference.

expressed as

$$\langle \Psi(t)_{\mathrm{pro(tar)}} | z | \Psi(t)_{\mathrm{pro(tar)}} \rangle$$
$$= \frac{1}{N_{\mathrm{pro(tar)}}} \sum_{i,j \in \mathrm{pro(tar)}} n_{i,j} \langle \psi_i(t) | z | \psi_j(t) \rangle, \qquad (12)$$

where $N_{\mathrm{pro(tar)}}$ is the particle number of the projectile (target), and i and j are indices belonging to the projectile or the target. The expectation values of other one-body operators, like the total momentum $P_{\mathrm{pro(tar)}}$ mentioned later, are calculated in the same way.

As long as a one-to-one correspondence between R and t exists in the fusion process, we can label the state Ψ as well as the collective variables as a function of R instead of t. For instance, the variables of collective momenta, collective kinetic energy, and collective potential energy can all be expressed as a function of R:

$$P(R) = P_{\mathrm{pro}} - P_{\mathrm{tar}}, \qquad (13)$$

$$T_{\mathrm{coll}}(R) = \frac{P_{\mathrm{pro}}^2(R)}{2M_{\mathrm{pro}}} + \frac{P_{\mathrm{tar}}^2(R)}{2M_{\mathrm{tar}}}, \qquad (14)$$

$$V_{\mathrm{coll}}(R) = E_{\mathrm{tot}}(R) - E_{\mathrm{pro}}(R) - E_{\mathrm{tar}}(R), \qquad (15)$$

where P_{pro} and P_{tar} are the total momentum of projectile and target calculated in the same way as Eq. (12); M_{pro} and M_{tar} are the total mass of projectile and target; E_{tot} is the total energy of the whole system and E_{pro} and E_{tar} are the total energies of the projectile and target.

Figure 2 shows the collective potential energy defined in Eq. (15) along the reaction path of the fusion reaction $^{16}\mathrm{O} + ^{16}\mathrm{O} \rightarrow ^{32}\mathrm{S}$ as a function of relative distance R. At large distances, the collective potential agrees with the asymptotic Coulomb potential, $V_{\mathrm{coll}} \approx Z^2 e^2/R$, shown with a dashed (green) line for reference. Overcoming the Coulomb barrier at $R = 8.3$ fm, the collective potential monotonically decreases as the nuclei come closer together and fuse. The red and blue curves indicate two different incident energies of $E_{\mathrm{c.m}} =$

20 MeV and $E_{\mathrm{c.m.}} = 40$ MeV, respectively. The difference in collective potentials at the two incident energies is at most of 20 MeV in the region $2.5 < R < 7.5$ fm. We find that the results at a higher incident energy are higher than those at lower incident energy. As studied in Refs. [25,26], this is due to the different rate of rearrangement among the intrinsic degrees of freedom between the fast and slow collision. The differences between the TDHF and TDDM approaches are much smaller than those associated with the incident energy. The THDF collective potential is within 5 MeV of the TDDM potential for all positions and energies. This indicates a relatively small effect of two-body dissipation on the collective potentials in this reaction.

The intrinsic energy

$$E_{\mathrm{intr}}(R) = E_{\mathrm{c.m.}} - E_{\mathrm{coll}}(R) \qquad (16)$$

is obtained by subtracting the collective energy, $E_{\mathrm{coll}}(R) = T_{\mathrm{coll}}(R) + V_{\mathrm{coll}}(R)$, from the the initial bombarding energy in the center-of-mass coordinate frame. To define the friction force F_{fric}, we assume that all the work done by this force is converted into intrinsic energy. Under this assumption, the friction force can be extracted as the derivative with respect to the R collective variable of the intrinsic energy,

$$F_{\mathrm{fric}}(R) = \frac{dE_{\mathrm{intr}}(R)}{dR}. \qquad (17)$$

According to the Rayleigh formula [27,47], the friction coefficient $\gamma(R)$ as a function of R is extracted from the ratio

$$\gamma(R) = \frac{F_{\mathrm{fric}}(R)}{P(R)}, \qquad (18)$$

with $P(R)$ defined as in Eq. (13).

III. APPLICATION

In this section we apply the macroscopic reduction procedure to investigate the dissipation mechanism of the reaction $^{16}\mathrm{O} + ^{16}\mathrm{O} \rightarrow ^{32}\mathrm{S}$. The method to conserve the total energy within the TDDM$^{\mathrm{P}}$ scheme introduced above is incorporated in the calculation. The TDDM$^{\mathrm{P}}$ dynamics is built on top of the SKY3D code [48], which solves the TDHF equations on a three-dimensional Cartesian mesh with Skyrme forces [43,44]. To solve Eqs. (6)–(8), a fourth-order Runge-Kutta time propagation algorithm is used to improve the accuracy of the solution and the convergence of the initial states.

We adopt the Skyrme III force to calculate mean-field component of the interaction matrix as well as the mean-field Hamiltonian in Eq. (8) [49]. Skyrme III is a standard parametrization of the Skyme force, in which the density dependent term as well as the spin-orbit term are present. The residual interaction is assumed to be of zero-range with a linear density dependence following the standard choice in the literature [38,50–52],

$$v_{12}(\vec{r}_1, \vec{r}_2) = v_0 \left[1 - \frac{\rho(r)}{\rho_0} \right] \delta(\vec{r}_1 - \vec{r}_2), \qquad (19)$$

where $\rho(r)$ is the nuclear density and $\rho = 0.16$ fm^{-3} is the saturation density. The strength of the residual interaction v_0 is set to be -1200 MeV fm^3, following Ref. [50]. We discretize
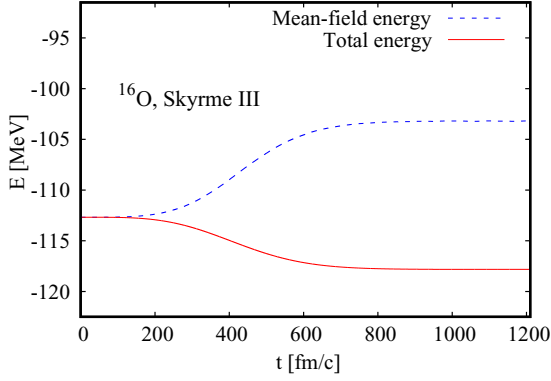
FIG. 3. Solid line: the total energy of ^{16}O as it evolves from the Hartree-Fock state to the TDDM correlated state by switching on the residual interaction adiabatically. Dashed line: the mean-field energy in the same conditions. This figure is obtained with $N_{max} = 30$.

the mesh in a cubic box of size $16.5 \times 16.5 \times 16.5$ fm^3 for the preparation of the projectile and target, and a rectangular box of size $16.5 \times 16.5 \times 33.0$ fm^3 for the reaction. The mesh spacing is set to $\Delta x = 1.1$ fm in all directions. The time step is $\Delta t = 0.3$ fm/c. All simulations are run for a total time of 150 fm/c.

A. Correlated ground state of ^{16}O

The initial correlated ground states of the projectile and target are generated by means of the adiabatic switching technique [53]. A static Hartree-Fock (HF) calculation is performed first to obtain an initial mean-field ground state. Starting from this HF state, we switch on the residual interaction of Eq. (19) adiabatically. The time-dependent residual interaction is given by the expression

$$v_{12}(\vec{r}_1, \vec{r}_2, t) = \left(1 - e^{-\frac{t^2}{\tau^2}}\right) v_{12}(\vec{r}_1, \vec{r}_2), \qquad (20)$$

which satisfies $v_{12}(\vec{r}_1, \vec{r}_2, t = 0) = 0$ and $v_{12}(\vec{r}_1, \vec{r}_2, t \to \infty) = v_{12}$. While the residual interaction is switched on, we evolve the system following the TDDM^P equations (1), (6), and (7). In order to obtain a stationary correlated state, the adiabatic theorem requires the interaction to be switched on slowly enough. For ^{16}O, we find that setting $\tau = 300$ fm/c provides a good compromise.

To obtain the correlated ground state of ^{16}O, different schemes for model spaces have been proposed in the TDDM model [38]. In this work, we use a model space consisting of $N_{max} = 30$ orbits, with $N_{max}^n = 16$ neutron states and $N_{max}^p = 14$ proton states, so that all these single-particle states are kept bound and evaporation is avoided during the fusion process.

Figure 3 shows the evolution of the total energy (solid line) with time as the residual interaction is switched on following Eq. (20). The dashed (blue) curve indicates the energy without two-body correlations. The initial system is uncorrelated and the total energy is entirely due to the mean-field contribution. As the residual interaction is switched on, the system becomes more bound by about 5.2 MeV. The mean-field contribution, in contrast, is about 9.5 MeV less attractive, mostly due to the increase in kinetic energy associated with correlations.

TABLE I. Converged occupation numbers, n_{ii}, of the single-particle states for ^{16}O. The calculation is performed with $N_{max} = 30$. The numbers in the parentheses denote the degeneracy of the corresponding orbits.

	$1s$ (2)	$1p_{3/2}(4)$	$1p_{1/2}(2)$	$1d_{5/2}(6)$	$2s(2)$
Neutron	0.988	0.954	0.887	0.068	0.013
Proton	0.992	0.962	0.907	0.059	

Both curves display a quite satisfactory convergence, indicating that, as we turn on correlations adiabatically, a stable correlated ground state is obtained. With the parameter set of Skyrme III for the mean-field part and Eq. (19) for the residual interaction, the final contribution of the two-body correlations to the total energy is about 14.7 MeV for the ground state of ^{16}O. We note that the total energy is conserved after convergence. In other words, $\beta(t)$ in Eq. (9) turns out to be zero if the moving basis of Eq. (8) is used. This is no longer true when the two nuclei collide, as shown in the next subsection.

Table I gives the occupation numbers, n_{ii}, of different single-particle orbits for the correlated ground state of ^{16}O. The deeply bound $1s_{1/2}$ and $1p_{3/2}$ neutron and proton states keep more than 95% of the single-particle occupation. Correlations have the largest effect near the Fermi surface, where they effectively deplete the $1p_{1/2}$ states by about 10% and allow for a 6–7% population of the $1d_{5/2}$ states. Neutron $2s_{1/2}$ orbits remain almost unpopulated. We note that in the TDDM method the strength of two-body correlation effects and single-particle occupations depend on the strength of the residual interaction. A systematic study on the correlated static state will be addressed in a separate work.

B. Dissipation with two-body correlations

In this subsection, we explore the dissipation dynamics of the reaction ^{16}O + ^{16}O → ^{32}S. The initial relative distance between the two correlated ground states of ^{16}O is set to be 10 fm. In the center-of-mass frame, we boost the projectile and target symmetrically by assigning an initial velocity to all the single-particle states. For the TDDM^P calculation, the numerical procedure introduced in Sec. III B is applied to the time evolution of the orbits. The occupation number and the correlation matrix evolve following Eqs. (6) and (7).

Figure 4(a) shows the friction coefficient γ, defined in Eq. (18), as a function of the relative distance R for a collision energy of $E_{c.m.} = 40$ MeV. The parameter β (bottom panel) of Eq. (9) is shown in Fig. 4(b). Since the one-to-one correspondence between R and t is valid during the collision, β is also expressed as a function of R instead of t. Curves of different styles indicate results calculated with different total number of orbits, N_{max}, for the total system. In other words, N_{max} here is the sum of N_{max} of both projectile and target. The initial ground states of ^{16}O are thus constructed using $N_{max}/2$ orbits with $N_{max}^n = N_{max}^p = N_{max}/4$. As N_{max} increases, we find that both β and γ converge in the region $R < 8$ fm. We take this as an indication of numerical convergence over the basis size in the region where the two nuclei are in contact with each other.

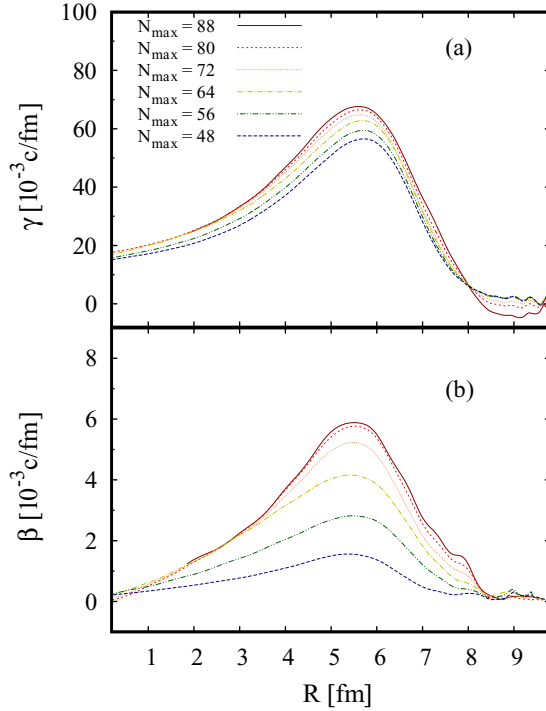FIG. 4. (a) Friction coefficient γ as a function of R for the fusion reaction $^{16}O + {}^{16}O \rightarrow {}^{32}S$ at $E_{\text{c.m.}} = 40$ MeV. Different line styles indicate results calculated with different N_{max}. (b) β parameters in the same conditions.

FIG. 5. Intrinsic energy as a function of R. The solid and dotted lines indicate the results of TDDM and TDHF simulations, respectively. The blue (upper) and red (lower) lines indicate the results at incident energies of $E_{\text{c.m.}} = 20$ MeV and $E_{\text{c.m.}} = 40$ MeV, respectively.

Before the two nuclei overlap at $R > 8$ fm, for $N_{\text{max}} > 80$, the results are less stable and negative friction can appear. This is a discretization artifact, as several single-particle states are unbound when $N_{\text{max}} > 80$.

At large distances, $R > 8.5$ fm, the friction coefficients in Fig. 4(a) are asymptotically zero. This indicates that the two nuclei keep their ground state properties in the approaching phase. As the two nuclei start to overlap, γ first increases to $\gamma \approx 65$ c/fm at $R \approx 5.5$ fm, and subsequently decreases to a value of $\gamma \approx 18$ c/fm as $R \rightarrow 0$. The hump peak at intermediate distances corresponds to the region where collective motion is most damped. The position of the peak turns out to depend on the incident energy, as will be shown below. The shape of the friction coefficient curve qualitatively agrees with the calculations of the DD-TDHF method [25,26].

The dependence on R of the β coefficient is very similar. At large distances $R > 8.5$ fm, $\beta = 0$, indicating that the total energy can be conserved without the additional term v' in Eq. (1). As the two nuclei overlap at distances below $R = 8.5$ fm, β starts to grow. $\beta(R)$ presents a maximum that coincides with the maximum of $\gamma(R)$. This may imply that, in a conventional TDDM^P calculation, a finite basis may cause inadequate dissipation. Unlike γ, when the system gets more compact as R decreases, β reduces to zero again. Our results thus indicate that energy nonconserving effects are maximal in the region after contact, when the collective motion in the compound nucleus is more strongly damped. We note that β is positive throughout the evolution, which indicates that
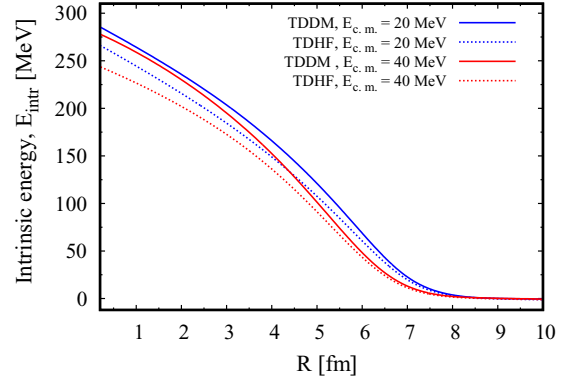
the energy-conserving dynamics is preferentially reducing the momentum of single-particle states.

The results in Fig. 4 validate the strategy discussed in Sec. III B. The convergence is achieved as the basis size increases. The physical γ friction coefficient is relatively insensitive to the total basis size compared to β. The maximum value of γ increases by less than 21% when going from $N_{\text{max}} = 48$ to $N_{\text{max}} = 88$. In contrast, the adjusted parameter β is more sensitive to the model space and increases by a factor of 4. We note that $\beta \neq 0$ even with the very large basis sizes explored here, which means the violation of energy conservation in this implementation of TDDM cannot be remedied by increasing the number of moving orbits.

We now turn to look at the effect of two-body collisions in the dissipation processes. For comparison, we simulate the reaction at two different incident energies $E_{\text{c.m}} = 20$ MeV and $E_{\text{c.m}} = 40$ MeV, with TDDM^P and TDHF, using the same underlying mean-field interaction. The TDDM^P dynamics are computed with $N_{\text{max}} = 60$. Figure 5 shows the intrinsic energy defined in Eq. (16) as a function of R for both TDHF and TDDM^P simulations at the two incident energies. At large distance, a zero intrinsic energy indicates again that the two nuclei remain close to the ground state in the approaching phase. After contact, the intrinsic energy grows monotonically in the region $R < 8$ fm all the way to values of $E_{\text{intr}} \approx 250$–300 MeV at $R \rightarrow 0$. Compared with the evolution at $E_{\text{c.m.}} = 20$ MeV, the dissipation processes at $E_{\text{c.m.}} = 40$ MeV start relatively later. A nonzero value of E_{intr} appears at a smaller R at $E_{\text{c.m.}} = 40$ MeV, corresponding to a more compact configuration. This feature of retarded dissipation has been studied in TDHF [25]. For the TDHF simulations, the curves at $E_{\text{c.m.}} = 20$ MeV and $E_{\text{c.m.}} = 40$ MeV increase at very similar rates. For TDDM^P, E_{intr} grows faster at higher collision energy in the interior region $R < 4$ fm. We take the difference between TDDM^P and TDHF intrinsic energies as an indication of dissipation stemming from two-body correlations. The results in Fig. 5 suggest that the higher the incident energy is, the more energy is dissipated from two-body collisions. This effect can be
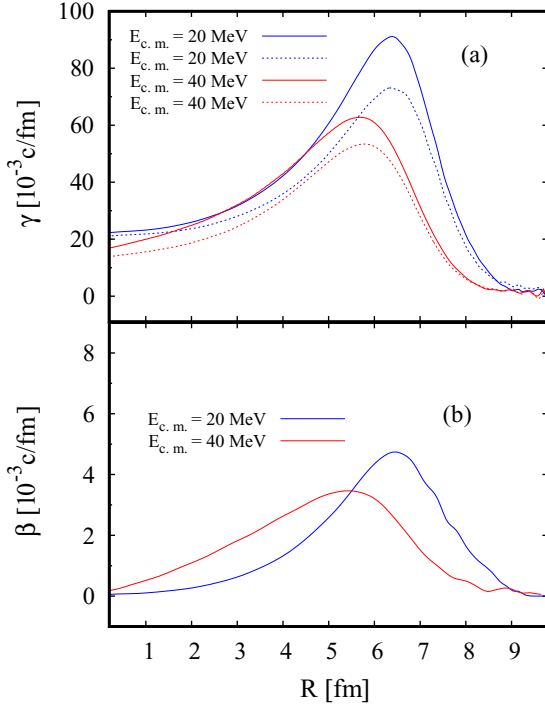
FIG. 6. (a) Friction coefficient γ for TDDM^P (solid lines) and TDHF (dotted lines) simulations as a function of R. Blue (upper) and red (lower) lines indicate the results at incident energies of $E_{c.m.} = 20$ MeV and $E_{c.m.} = 40$ MeV, respectively. (b) β parameters in the same conditions.

further quantified by looking at the friction coefficient and the β parameter.

Figure 6(a) shows the friction coefficient γ obtained in TDDM^P (solid lines) and TDHF (dotted lines) simulations. The parameter β in the TDDM^P simulations is shown in Fig. 6(b). The shapes of the friction coefficients as a function of R are very similar for both the TDDM^P and the TDHF simulations. At large R, there is no active dissipation at either energy, so $\gamma = 0$. As R decreases, the friction coefficients develop a hump. The position and size of the maximum changes depending on incident energy and the treatment of two-body dissipation. The lower incident energies correspond to larger maxima at larger separations. For instance, for TDDM^P at $E_{c.m.} = 20$ MeV, the peak value is $\gamma = 86$ c/fm at $R = 6.5$ fm, whereas at $E_{c.m.} = 40$ MeV the corresponding maximum friction coefficient is $\gamma = 64$ c/fm at $R = 5.7$ fm. Thus, friction is more effective at lower incident energies.

It is in the peak region of γ that the largest differences between the treatments of correlations are found. γ_{TDDM} is about 20% larger than γ_{TDHF} for the two incident energies considered here. This shows that two-body correlations contribute to enhance dissipation effects. The increase in γ due to two-body collisions is more significant at lower incident energy. This is at odds with the discussion around Fig. 5, which indicated that, in terms of intrinsic excitation energy, two-body correlations contribute more at higher energies. The friction coefficient is, however, inversely proportional to the collective momentum; it therefore probes the time dependence of the reaction in a

more sensitive way. This energy dependence also agrees with the results obtained in DD-TDHF calculations [25,26]. We note that as R becomes smaller and the compound nucleus contracts, friction becomes less important. In the region where $R \lesssim 3$ fm, all the results flatten out to values $\gamma \approx 20$ c/fm.

The results for $\beta(R)$ are shown in Fig. 6(b). The values of β are one order of magnitude smaller than those of γ. β is very close to zero both at large R and small R. It is positive at both incident energies and develops a clear maximum as a function of R. At lower (higher) energies, the maximum is larger (lower), with $\beta \approx 4.8$ c/fm ($\beta \approx 3.6$ c/fm) at $R \approx 6.5$ fm ($R \approx 5.7$ fm). The position of the maximum of β coincides with that of γ at both incident energies. We take this as an indication that two-body dissipative effects are maximal at the point where the incompleteness of the basis is more critical.

Finally, we comment on the absolute values of both γ and β. Maximum values of γ are about a factor of 20 larger than maximum values of β. Both quantities have the same units and represent, in some way, inverse timescales associated with dissipation. γ can be thought of as the inverse timescale associated with dissipative friction effects. One can interpret β as the inverse timescale associated with basis incompleteness (or any other mechanism) bringing in energy nonconservation. The very small values of β indicate that dissipation is governed by the relatively faster friction processes, whereas any energy nonconserving effects set in later in the dynamics. We therefore expect that our results will hold in all implementations of TDDM, independently of whether an incomplete moving basis is used or not.

IV. SUMMARY

In this work, we study the fusion dynamics of light nuclei using time-dependent simulations. We are interested in quantifying the effect of dissipative effects beyond the mean-field level. To this aim, we implement TDHF and TDDM^P simulations of the the nuclear fusion reaction ^{16}O + ^{16}O $\rightarrow$ ^{32}S. We propose a method to remedy the problem of energy nonconservation in the TDDM approach. The method is based on the idea that the finite moving basis in which the TDDM dynamics is described can be optimized by introducing a correction term in the mean-field Hamiltonian. With conservation of energy restored, we apply a macroscopic reduction procedure to TDDM simulations to study the dissipation mechanisms. The friction coefficients are extracted for both TDHF and TDDM calculations. We find that the size of the basis does not qualitatively affect the determination of the TDDM friction coefficients.

Compared to the results of TDHF dynamics, where two-body correlations are absent, we find that dissipation is enhanced noticeably in TDDM simulations. For instance, the friction coefficients in TDDM dynamics can be up to 20% larger than TDHF results. We also find that at higher bombarding energy, two-body correlations provide a larger contribution to dissipation than at lower energy.

The form of interaction is critical in TDDM simulations, and could play an important role in the dissipation process. In this work, we use Skyrme III to construct the mean-field in the TDHF and TDDM calculations. We have used a generalized pairing and surface-dominated interaction under

the TDDM^P approximation. The work presented here is the first investigation in this direction, but the choice of the interaction remains ambiguous. A more thorough analysis of how both the mean-field and the residual interactions affect these results would be a first step beyond this work. A systematic study of the dissipation process for different reaction systems is also under way.

[1] D. Brink, *Semi-Classical Methods for Nucleus-Nucleus Scattering* (Cambridge University Press, Cambridge, 1985).

[2] W. U. Schröder and J. R. Huizenga, in *Teatise on Heavy-Ion Science*, edited by D. A. Bromley (Plenum, New York, 1984).

[3] J. Blocki, Y. Boneh, J. R. Nix, J. Randrup, M. Robel, A. J. Sierk, and W. J. Swiatecki, Ann. Phys. (NY) **113**, 330 (1978).

[4] H. Feldmeier, Rep. Prog. Phys. **50**, 915 (1987).

[5] S. Bjørnholm and W. J. Swiatecki, Nucl. Phys. A **391**, 471 (1982).

[6] Y. Abe, S. Ayik, P.-G. Reinhard, and E. Suraud, Phys. Rep. **275**, 49 (1996).

[7] D. Lacroix, S. Ayik, and P. Chomaz, Prog. Part. Nucl. Phys. **52**, 497 (2004).

[8] D. Lacroix, arXiv:nucl-th/0202063.

[9] K. Siwek-Wilczyńska, T. Cap, M. Kowal, A. Sobiczewski, and J. Wilczyński, Phys. Rev. C **86**, 014611 (2012).

[10] K. Wen, F. Sakata, Z.-X. Li, X.-Z. Wu, Y.-X. Zhang, and S.-G. Zhou, Phys. Rev. Lett. **111**, 012501 (2013).

[11] P. Bonche, S. Koonin, and J. W. Negele, Phys. Rev. C **13**, 1226 (1976).

[12] L. Guo, J. A. Maruhn, P.-G. Reinhard, and Y. Hashimoto, Phys. Rev. C **77**, 041301 (2008).

[13] C. Simenel, B. Avez, and D. Lacroix, arXiv:0806.2714.

[14] C. Simenel, Eur. Phys. J. A **48**, 152 (2012).

[15] A. Bulgac, Ann. Rev. Nucl. Part. Sci. **63**, 97 (2013).

[16] T. Nakatsukasa, K. Matsuyanagi, M. Matsuo, and K. Yabana, Rev. Mod. Phys. **88**, 045004 (2016).

[17] R. Y. Cusson, P. G. Reinhard, M. R. Strayer, J. A. Maruhn, and W. Greiner, Z. Phys. A **320**, 475 (1985).

[18] A. S. Umar and V. E. Oberacker, Phys. Rev. C **74**, 021601 (2006).

[19] R. Keser, A. S. Umar, and V. E. Oberacker, Phys. Rev. C **85**, 044606 (2012).

[20] C. Simenel, R. Keser, A. S. Umar, and V. E. Oberacker, Phys. Rev. C **88**, 024617 (2013).

[21] C. Simenel, M. Dasgupta, D. J. Hinde, and E. Williams, Phys. Rev. C **88**, 064604 (2013).

[22] C. Simenel, P. Chomaz, and G. de France, Phys. Rev. Lett. **93**, 102701 (2004).

[23] J. Randrup and W. Swiatecki, Ann. Phys. (NY) **125**, 193 (1980).

[24] J. Randrup and W. Swiatecki, Nucl. Phys. A **429**, 105 (1984).

[25] K. Washiyama, D. Lacroix, and S. Ayik, Phys. Rev. C **79**, 024609 (2009).

[26] K. Washiyama and D. Lacroix, Phys. Rev. C **78**, 024610 (2008).

[27] S. Ayik, K. Washiyama, and D. Lacroix, Phys. Rev. C **79**, 054606 (2009).

[28] H. Born and H. Green, Proc. R. Soc. London, Ser. A **188**, 10 (1946); N. N. Bogoliubov, J. Phys. USSR **10**, 265 (1946); J. G. Kirkwood, J. Chem. Phys. **14**, 180 (1946).

[29] P. Ring and P. Schuck, in *The Nuclear Many-Body Problem*, edited by N. York (Springer, Berlin, 1980).

[30] M. Gong, Ph.D. thesis, Michigan State University, 1990 (unpublished).

[31] A. Akbari, M. J. Hashemi, A. Rubio, R. M. Nieminen, and R. van Leeuwen, Phys. Rev. B **85**, 235121 (2012).

[32] A. Akbari, Ph.D. thesis, University of the Basque Country, 2012 (unpublished).

[33] M. Tohyama, Phys. Rev. C **91**, 017301 (2015).

[34] W. Shun-jin and W. Cassing, Ann. Phys. (NY) **159**, 328 (1985).

[35] K.-J. Schmitt, P.-G. Reinhard, and C. Toepffer, Z. Phys. A **336**, 123 (1990).

[36] M. Tohyama, Phys. Rev. C **36**, 187 (1987).

[37] M. Tohyama, Prog. Theor. Phys. **92**, 905 (1994).

[38] M. Tohyama and A. Umar, Phys. Lett. B **549**, 72 (2002).

[39] M. Tohyama and A. S. Umar, Phys. Rev. C **93**, 034607 (2016).

[40] C.-Y. Wong and H. H. K. Tang, Phys. Rev. Lett. **40**, 1070 (1978).

[41] S. E. Koonin, Prog. Part. Nucl. Phys. **4**, 283 (1980).

[42] H. Appel and E. K. U. Gross, Europhys. Lett. **92**, 23001 (2010).

[43] M. C. Barton, Ph.D. thesis, University of Surrey, 2018 (unpublished).

[44] M. C. Barton, P. D. Stevenson, and A. Rios (unpublished).

[45] M. Assié, Ph.D. thesis, Université de Paris-Sud, Paris 11, 2008 (unpublished).

[46] M. Assié and D. Lacroix, Phys. Rev. Lett. **102**, 202501 (2009).

[47] P. Fröbrich and I. I. Gontchar, Phys. Rep. **292**, 131 (1998).

[48] J. Maruhn, P.-G. Reinhard, P. Stevenson, and A. Umar, Comput. Phys. Commun. **185**, 2195 (2014).

[49] M. Beiner, H. Flocard, N. Van Giai, and P. Quentin, Nucl. Phys. A **238**, 29 (1975).

[50] R. R. Chasman, Phys. Rev. C **14**, 1935 (1976).

[51] M. Yamagami, K. Matsuyanagi, and M. Matsuo, Nucl. Phys. A **693**, 579 (2001).

[52] T. Duguet, P. Bonche, and P.-H. Heenen, Nucl. Phys. A **679**, 427 (2001).

[53] A. Rios, B. Barker, M. Buchler, and P. Danielewicz, Ann. Phys. (NY) **326**, 1274 (2011).